

# RSC Advances



This is an *Accepted Manuscript*, which has been through the Royal Society of Chemistry peer review process and has been accepted for publication.

*Accepted Manuscripts* are published online shortly after acceptance, before technical editing, formatting and proof reading. Using this free service, authors can make their results available to the community, in citable form, before we publish the edited article. This *Accepted Manuscript* will be replaced by the edited, formatted and paginated article as soon as this is available.

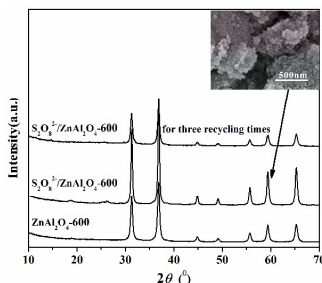
You can find more information about *Accepted Manuscripts* in the [Information for Authors](#).

Please note that technical editing may introduce minor changes to the text and/or graphics, which may alter content. The journal's standard [Terms & Conditions](#) and the [Ethical guidelines](#) still apply. In no event shall the Royal Society of Chemistry be held responsible for any errors or omissions in this *Accepted Manuscript* or any consequences arising from the use of any information it contains.

A table of contents entry

## A novel solid acid catalyst synthesized from $\text{ZnAl}_2\text{O}_4$ spinel and its application in esterification of acetic acid and *n*-butyl alcohol.

An-Qi Wang,<sup>a</sup> Xiu-Ling Wu,<sup>a</sup> Jun-Xia Wang,<sup>\*a</sup> Hui Pan,<sup>a</sup> Xiao-Yun Tian<sup>a</sup> and Yu-Lin Xing<sup>a</sup>



A new spinel-style  $\text{S}_2\text{O}_8^{2-}/\text{ZnAl}_2\text{O}_4$  catalyst with the mesoporous structure exhibited the well catalytic activity and structural stability.

Cite this: DOI: 10.1039/c0xx00000x

www.rsc.org/xxxxxx

ARTICLE TYPE

# A novel solid acid catalyst synthesized from ZnAl<sub>2</sub>O<sub>4</sub> spinel and its application in esterification of acetic acid and *n*-butyl alcohol.

An-Qi Wang,<sup>a</sup> Xiu-Ling Wu,<sup>a</sup> Jun-Xia Wang,<sup>\*a</sup> Hui Pan,<sup>a</sup> Xiao-Yun Tian<sup>a</sup> and Yu-Lin Xing<sup>a</sup>

<sup>5</sup> Received (in XXX, XXX) Xth XXXXXXXXXX 20XX, Accepted Xth XXXXXXXXXX 20XX

DOI: 10.1039/b000000x

**Abstract:** A new spinel-style S<sub>2</sub>O<sub>8</sub><sup>2-</sup>/ZnAl<sub>2</sub>O<sub>4</sub> solid acid catalyst was prepared by sol-gel method. The catalytic performance was evaluated by the esterification of *n*-butyl acetate. The structure, morphology and acidity of the samples were characterized by X-ray diffraction (XRD), Fourier transform infrared spectroscopy (FT-IR), Field emission scanning electron microscopy (FE-SEM), N<sub>2</sub> physisorption, X-ray photoelectron spectroscopy (XPS) and NH<sub>3</sub> temperature programmed desorption (NH<sub>3</sub>-TPD). The results showed that the catalytic performances were significantly affected by the calcination temperature. The S<sub>2</sub>O<sub>8</sub><sup>2-</sup>/ZnAl<sub>2</sub>O<sub>4</sub>-600 exhibited the highest catalytic activity of 91.7% under the optimum reaction conditions. The characterization showed that the mesoporous structure S<sub>2</sub>O<sub>8</sub><sup>2-</sup>/ZnAl<sub>2</sub>O<sub>4</sub>-600 maintained the well crystallinity of spinel as well as the spinel-style carrier in the sulfidation and recycling.

## 1. Introduction

The esterification of carboxylic acids with alcohols is an essential reaction in organic synthesis, pharmaceuticals, food preservatives, biofuels, etc. Two representative catalysts of SO<sub>4</sub><sup>2-</sup>/ZrO<sub>2</sub> and SO<sub>4</sub><sup>2-</sup>/TiO<sub>2</sub> are widely used in these esterifications, due to their strong acidity, non-toxicity and high catalytic activity.<sup>1,2</sup> However, they have a similar problem in the crystal structure transformation in the process of synthesis and modification.<sup>3,4</sup> It is well known that the crystal structure of metal oxide has a great influence on the catalytic performances.<sup>5</sup> Therefore, it is desirable for researchers to look for a stable carrier to synthesize solid acid. Spinel-type oxide has drawn great attention for catalytic reactions because of its desirable properties, such as single crystal shape, high thermal stability and well diffusion, etc.<sup>6-9</sup> A nanosized sulfated ZnFe<sub>2</sub>O<sub>4</sub> catalyst with highly ordered mesoporous was found to be highly active towards commercially important fine chemicals.<sup>10</sup> The high specific surface area SO<sub>4</sub><sup>2-</sup>/CoFe<sub>2</sub>O<sub>4</sub> solid acid with the spinel as carrier displayed the excellent activity in the synthesis of ethyl acetate.<sup>11</sup> Nevertheless, the literature on the catalytic applications of S<sub>2</sub>O<sub>8</sub><sup>2-</sup>/ZnAl<sub>2</sub>O<sub>4</sub> catalyst is scanty. In our previous studies, the composite catalysts of Al-based catalysts have been developed and studied in terms of the catalytic activity and reusability, which performed the high catalytic activity and excellent stability.<sup>12-14</sup> Therefore, the ZnAl<sub>2</sub>O<sub>4</sub> spinel may be a promising carrier for solid acid.

In this work, a series of S<sub>2</sub>O<sub>8</sub><sup>2-</sup>/ZnAl<sub>2</sub>O<sub>4</sub>-*T* were prepared and evaluated by the esterification of *n*-butyl acetate. The influences of synthesis conditions on the catalytic activities were studied. In addition, the reaction conditions and catalyst recyclability were also performed in detail. Furthermore, the structure, morphology and acidity of the catalyst were characterized by XRD, FE-SEM, N<sub>2</sub> physisorption, FT-IR, NH<sub>3</sub>-TPD and XPS techniques. Some

valuable evaluations for the S<sub>2</sub>O<sub>8</sub><sup>2-</sup>/ZnAl<sub>2</sub>O<sub>4</sub> in this paper have some referential value in the design of a novel ZnAl<sub>2</sub>O<sub>4</sub> carrier for SO<sub>4</sub><sup>2-</sup>/M<sub>x</sub>O<sub>y</sub> solid acid synthesis.

## 2. Experimental

### 2.1 Catalysts preparation

S<sub>2</sub>O<sub>8</sub><sup>2-</sup>/ZnAl<sub>2</sub>O<sub>4</sub> solid acid catalysts were prepared by the following steps: 0.04 mol Al(NO<sub>3</sub>)<sub>3</sub>·9H<sub>2</sub>O and 0.02 mol Zn(NO<sub>3</sub>)<sub>2</sub>·6H<sub>2</sub>O were dissolved in 20 mL ethyl alcohol, followed by adding 5 wt% (the total weight of nitrates) polyethylene glycol (PEG-2000) into the ethyl alcohol solution with magnetic stirring for 4 h at room temperature. Afterward, the obtained mixture was evaporated for 1 h at 60 °C to obtain the sol. The sol was dried and then grounded into a fine powder. The fine powder was calcined at 400°C, 500°C, 550°C, 600°C and 650 °C for 5 h in air to obtain the precursors. The obtained precursors with different calcination temperature were designated as ZnAl<sub>2</sub>O<sub>4</sub>-*T*. The ZnAl<sub>2</sub>O<sub>4</sub>-*T* were then sulfated for 12 h by impregnating with 0.75 mol/L, 1.00 mol/L, 1.25 mol/L, 1.50 mol/L, 1.75 mol/L and 2.00 mol/L (NH<sub>4</sub>)<sub>2</sub>S<sub>2</sub>O<sub>8</sub> solution. The sulfidation was done by impregnating 1 g of ZnAl<sub>2</sub>O<sub>4</sub> in 10 ml of (NH<sub>4</sub>)<sub>2</sub>S<sub>2</sub>O<sub>8</sub> solution for 12 hours. After having been filtered and dried, the solids were calcined at 550 °C for 5 h in air to obtain the S<sub>2</sub>O<sub>8</sub><sup>2-</sup>/ZnAl<sub>2</sub>O<sub>4</sub>-*T* catalysts. The S<sub>2</sub>O<sub>8</sub><sup>2-</sup>/ZnO-600 and S<sub>2</sub>O<sub>8</sub><sup>2-</sup>/Al<sub>2</sub>O<sub>3</sub>-600 catalysts were synthesized by the same steps.

### 2.2 Catalysts characterization

The X-ray diffraction (XRD) was conducted on a Bruker AXS D8-Focus X diffractometer, using CuKα radiation at 40 kV and 40 mA; The Fourier transform infrared spectroscopy (FT-IR) spectra of the catalysts were recorded in the range of 400-4000

cm<sup>-1</sup> by a Nicolet 6700 IR spectrometer using the KBr pellet technique; the morphology was examined by using Field emission scanning electron microscopy (FE-SEM) on a SU 8010 electron microscope; The X-ray photoelectron spectroscopy (XPS) was performed on a VG Multilab 2000; The NH<sub>3</sub> temperature programmed desorption (NH<sub>3</sub>-TPD) experiment was carried out using a Micromeritics AutoChem II 2920 quipped with a TCD detector; N<sub>2</sub> adsorption analysis was carried out using micromeritics (ASAP-2020) at liquid nitrogen temperature (77 K). The surface area was calculated by the BET method and the pore size distribution was obtained from the adsorption isotherm by the BJH method.

### 2.3 Catalytic activity test

The esterification efficiency of *n*-butyl acetate was evaluated in a 250 mL three-necked flask equipped with a magnetic stirrer, a thermometer and a refluxing condenser. The mixture was stirred at about 118 °C under atmospheric pressure. Various parameters of the reaction conditions, including the molar ratio of *n*-butanol to acetic acid, catalyst amount (percentage content of the reaction mixture) and reaction time, were varied to the optimum. The initial acid and residual acid were detected by means of titration with 0.10 mol/L NaOH solution. The esterification efficiency of acetic acid can be calculated using the following equation (by the method of GB1668-81):

Esterification efficiency of acetic acid (%) =

$$\frac{M_0 - M_1}{M_0} \times 100$$

where  $M_0$  is the acid value before reaction and  $M_1$  is the acid value after reaction.

## 3. Results and discussion

### 3.1 Characterization of catalysts

Fig. 1 (a) shows the XRD patterns of ZnAl<sub>2</sub>O<sub>4</sub>-*T* and S<sub>2</sub>O<sub>8</sub><sup>2-</sup>/ZnAl<sub>2</sub>O<sub>4</sub>-*T*. It reveals that the calcination temperatures cause apparently changes in the crystalline structure of the carriers. The ZnAl<sub>2</sub>O<sub>4</sub>-400, ZnAl<sub>2</sub>O<sub>4</sub>-500 and ZnAl<sub>2</sub>O<sub>4</sub>-550 are mainly consisted of amorphous phase. When the calcinations temperature further increases, the amorphous gradually transforms into spinel. The characteristic peaks at  $2\theta = 18.9^\circ$ ,  $31.4^\circ$ ,  $36.90^\circ$ ,  $44.2^\circ$ ,  $49.2^\circ$ ,  $55.8^\circ$ ,  $59.5^\circ$  and  $65.4^\circ$  are observed ZnAl<sub>2</sub>O<sub>4</sub>-600 and ZnAl<sub>2</sub>O<sub>4</sub>-650, which are corresponding to the crystal planes of the spinel structure (JCPDS File No. 05-0669). Similar peaks are observed in S<sub>2</sub>O<sub>8</sub><sup>2-</sup>/ZnAl<sub>2</sub>O<sub>4</sub>-600 and S<sub>2</sub>O<sub>8</sub><sup>2-</sup>/ZnAl<sub>2</sub>O<sub>4</sub>-650, indicating that the spinel carriers have the excellent advantage of structure stability in sulfidation. Compared with the carriers, the crystallite size of S<sub>2</sub>O<sub>8</sub><sup>2-</sup>/ZnAl<sub>2</sub>O<sub>4</sub>-*T* is larger than ZnAl<sub>2</sub>O<sub>4</sub>-*T* as shown in Table 1. This result may be that the high calcination temperature in the process of sulfidation causes crystalline grain further to grow. Meanwhile, it can be found that the crystallite size gradually increases with increasing temperature. Besides, ZnSO<sub>4</sub>·H<sub>2</sub>O and Al<sub>2</sub>(SO<sub>4</sub>)<sub>3</sub> are observed in sulfated catalyst, which may be due to the long-time impregnation and the interaction between excess S<sub>2</sub>O<sub>8</sub><sup>2-</sup> and the metal ions.<sup>15,16</sup> Correlating the crystallization with the following catalytic

activities, the result shows that the spinel is an available carrier for solid acid.

Fig. 1 (b) clearly shows the XRD patterns of S<sub>2</sub>O<sub>8</sub><sup>2-</sup>/ZnAl<sub>2</sub>O<sub>4</sub>-600 with different impregnation concentration. It is noteworthy that all the catalysts appear the strong diffraction peaks of spinel (JCPDS File No. 05-0669). The well crystallization indicates that the spinel carrier perform the advantages of single crystal shape and stable structure with different impregnation concentration. Besides, the XRD patterns of used S<sub>2</sub>O<sub>8</sub><sup>2-</sup>/ZnAl<sub>2</sub>O<sub>4</sub>-600 in Fig. 1 (b) show no change in the crystallinity by comparing to the fresh catalyst, indicating the stable structure in recycling test.

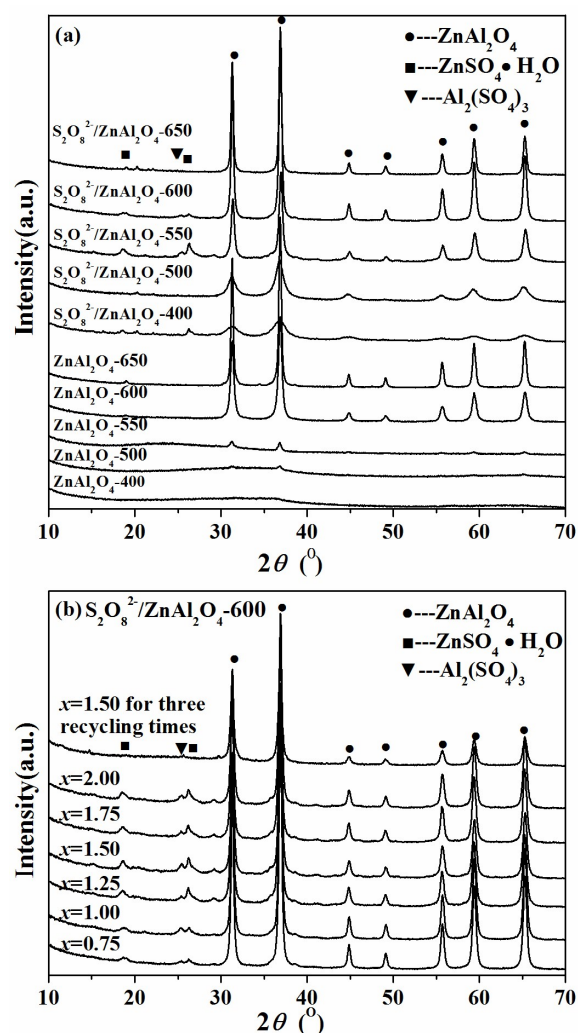


Fig. 1 XRD patterns of ZnAl<sub>2</sub>O<sub>4</sub>-*T* and S<sub>2</sub>O<sub>8</sub><sup>2-</sup>/ZnAl<sub>2</sub>O<sub>4</sub>-*T*: (a) different calcination temperature of carriers with 0.75 mol/L (NH<sub>4</sub>)<sub>2</sub>S<sub>2</sub>O<sub>8</sub> impregnating solution; (b) different concentration of (NH<sub>4</sub>)<sub>2</sub>S<sub>2</sub>O<sub>8</sub> solution.

Table 1 Crystallite sizes of ZnAl<sub>2</sub>O<sub>4</sub>-*T* and S<sub>2</sub>O<sub>8</sub><sup>2-</sup>/ZnAl<sub>2</sub>O<sub>4</sub>-*T*

	Crystallite size (nm) <sup>a</sup>				
	400	500	550	600	650
ZnAl <sub>2</sub> O <sub>4</sub> - <i>T</i>	/	/	7.23	17.99	25.82
S <sub>2</sub> O <sub>8</sub> <sup>2-</sup> /ZnAl <sub>2</sub> O <sub>4</sub> - <i>T</i> <sup>b</sup>	5.83	8.69	19.28	20.72	27.62

<sup>a</sup> From Debye-Scherrer equation using the width (at half maximum) of [3 0 1] line.

<sup>b</sup> the synthesis condition: calcination temperature was 600 °C; the concentration of  $(\text{NH}_4)_2\text{S}_2\text{O}_8$  solution was 1.50 mol/L.

FE-SEM images in Fig. 2 display the  $\text{S}_2\text{O}_8^{2-}/\text{ZnAl}_2\text{O}_4\text{-}T$  with different calcination temperatures. The irregular agglomerations are apparently appeared on the surfaces of  $\text{S}_2\text{O}_8^{2-}/\text{ZnAl}_2\text{O}_4\text{-}400$ ,  $\text{S}_2\text{O}_8^{2-}/\text{ZnAl}_2\text{O}_4\text{-}500$  and  $\text{S}_2\text{O}_8^{2-}/\text{ZnAl}_2\text{O}_4\text{-}650$ , which may be one reason of their low catalytic activities. The  $\text{S}_2\text{O}_8^{2-}/\text{ZnAl}_2\text{O}_4\text{-}550$  and  $\text{S}_2\text{O}_8^{2-}/\text{ZnAl}_2\text{O}_4\text{-}600$  show the morphology with flat blocks. By comparison,  $\text{S}_2\text{O}_8^{2-}/\text{ZnAl}_2\text{O}_4\text{-}600$  is composed of porous structures, which is assembled by numerous nanoparticles. Similarly, the fresh  $\text{S}_2\text{O}_8^{2-}/\text{ZnAl}_2\text{O}_4\text{-}600$  (Fig. 2(f)), impregnated with 1.50 mol/L  $(\text{NH}_4)_2\text{S}_2\text{O}_8$  solution, performs the porous structures. Correspondingly, the specific surface area, mean pore diameter and pore volumes are investigated by  $\text{N}_2$  adsorption analysis in Fig 3. The  $\text{N}_2$  adsorption/desorption isotherms correspond to the IV isotherm with a hysteresis loop in the low relative ( $P/P_0$ ) range of 0.4–1, which are typical for mesoporous materials. The surface area and average pore diameter are 18.776  $\text{m}^2/\text{g}$  and 8.864 nm, respectively. Similar porous structures can be observed in high active  $\text{SO}_4^{2-}/\text{TiO}_2$  catalysts.<sup>5</sup> These porous structures of  $\text{S}_2\text{O}_8^{2-}/\text{ZnAl}_2\text{O}_4\text{-}600$  may be beneficial to its high catalytic activity. Besides, the used  $\text{S}_2\text{O}_8^{2-}/\text{ZnAl}_2\text{O}_4\text{-}600$  catalyst in Fig. 2(g) maintains the agglomerate nanoparticles as the fresh catalyst.

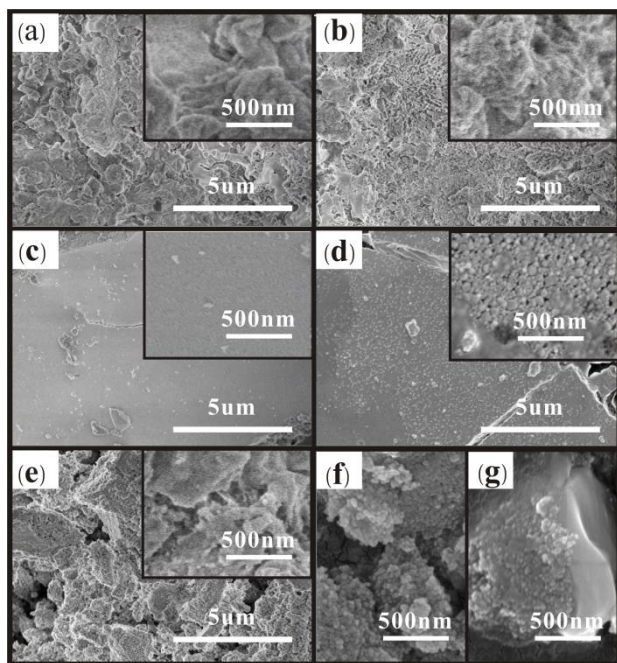


**Fig. 2** FE-SEM images of  $\text{S}_2\text{O}_8^{2-}/\text{ZnAl}_2\text{O}_4\text{-}T$ : (a)  $\text{S}_2\text{O}_8^{2-}/\text{ZnAl}_2\text{O}_4\text{-}400$ ; (b)  $\text{S}_2\text{O}_8^{2-}/\text{ZnAl}_2\text{O}_4\text{-}500$ ; (c)  $\text{S}_2\text{O}_8^{2-}/\text{ZnAl}_2\text{O}_4\text{-}550$ ; (d)  $\text{S}_2\text{O}_8^{2-}/\text{ZnAl}_2\text{O}_4\text{-}600$ ; (e)  $\text{S}_2\text{O}_8^{2-}/\text{ZnAl}_2\text{O}_4\text{-}650$ ; (f)  $\text{S}_2\text{O}_8^{2-}/\text{ZnAl}_2\text{O}_4\text{-}600$  (g)  $\text{S}_2\text{O}_8^{2-}/\text{ZnAl}_2\text{O}_4\text{-}600$  for three recycling times. ((a)–(e): 0.75 mol/L  $(\text{NH}_4)_2\text{S}_2\text{O}_8$  solution; (f) and (g): 1.50 mol/L  $(\text{NH}_4)_2\text{S}_2\text{O}_8$  solution.)

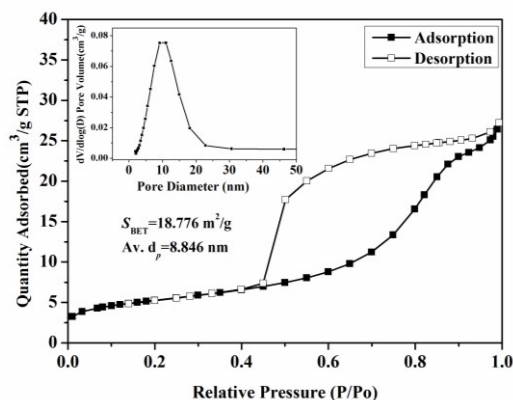


**Fig. 3**  $\text{N}_2$  adsorption-desorption isotherms and pore-size distributions of  $\text{S}_2\text{O}_8^{2-}/\text{ZnAl}_2\text{O}_4\text{-}600$ . (Impregnated with 1.50 mol/L  $(\text{NH}_4)_2\text{S}_2\text{O}_8$  solution)

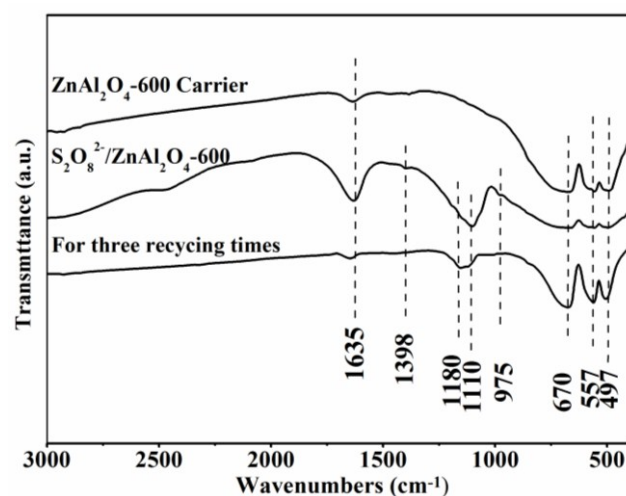


**Fig. 4** FT-IR spectra of  $\text{ZnAl}_2\text{O}_4\text{-}600$  carrier, fresh and used  $\text{S}_2\text{O}_8^{2-}/\text{ZnAl}_2\text{O}_4\text{-}600$  catalysts. (Impregnated with 1.50 mol/L  $(\text{NH}_4)_2\text{S}_2\text{O}_8$  solution.)

Fig. 4 records the FT-IR spectra of the  $\text{ZnAl}_2\text{O}_4\text{-}600$  carrier,  $\text{S}_2\text{O}_8^{2-}/\text{ZnAl}_2\text{O}_4\text{-}600$  solid acid catalyst and recycling catalyst. It can discern that three bands (around 672, 556 and 493  $\text{cm}^{-1}$ ) appeared in all the samples are consistent with characteristics of Al-O stretching vibrations, Zn-O stretching vibrations and Al-O bending vibrations in the crystal structure of  $\text{ZnAl}_2\text{O}_4$  spinel, respectively.<sup>17</sup> The result confirms that the spinel structure is formed in all the prepared samples, which is in agreement with the XRD analysis. Compared with  $\text{ZnAl}_2\text{O}_4\text{-}600$  carrier, there are distinguishing absorption peaks between 900 and 1400  $\text{cm}^{-1}$  in sulfated catalyst and recycling catalyst. The additional absorption peak characterizes the sulfate groups on the surface which are related to catalytic activity. The three bands at 982, 1103 and 1145  $\text{cm}^{-1}$  are assigned to the stretching vibration of S–O. The bands at 1220 and 1398  $\text{cm}^{-1}$  are assigned to the stretching vibration of S=O.<sup>18</sup> The existences of S=O and S–O bonds contribute to the coordination of the inorganic chelating bidentate sulfate ion with surface metal cation.<sup>19</sup> The recycling catalyst also displays the similar peaks belonged to spinel structure and sulfate groups, indicating that the  $\text{S}_2\text{O}_8^{2-}/\text{ZnAl}_2\text{O}_4\text{-}600$  catalyst has the advantage of structure stability in recycling test. This result is in agreement with the XRD analysis. In addition, the band around

1627  $\text{cm}^{-1}$  is assigned to the bending modes of the  $-\text{OH}$  group.

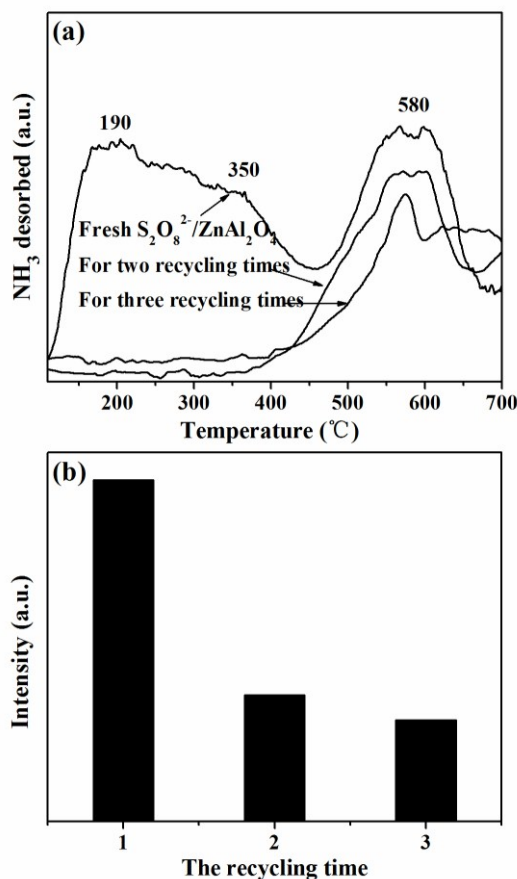


Fig. 5  $\text{NH}_3$ -TPD curves and areas for fresh and used  $\text{S}_2\text{O}_8^{2-}/\text{ZnAl}_2\text{O}_4$ -600. (Impregnated with 1.50 mol/L  $(\text{NH}_4)_2\text{S}_2\text{O}_8$  solution)

As shown in Fig.5 (a), the acid strength distributions of  $\text{S}_2\text{O}_8^{2-}/\text{ZnAl}_2\text{O}_4$ -600 and reused catalysts are characterized by the  $\text{NH}_3$ -TPD. The higher of desorption peak temperature represents the stronger of the acid strength. The fresh  $\text{S}_2\text{O}_8^{2-}/\text{ZnAl}_2\text{O}_4$ -600 catalyst shows prominent broad peaks in the range of 100  $^\circ\text{C}$  to 700  $^\circ\text{C}$ , indicating a wide distribution of acidic sites. The two peaks around 190  $^\circ\text{C}$  and 350  $^\circ\text{C}$  correspond to the acidic site of weak and medium strength, respectively.<sup>20</sup> The peak above 500  $^\circ\text{C}$  assigns to strong acidic site.<sup>21</sup> The area of the  $\text{NH}_3$  desorption curve shown in Fig.5 (b) is in proportion to the content of the corresponding acid sites. It is clearly found that the number of acid sites decreases in the used catalysts, which may be the one of reasons for its deactivation in recycling test.

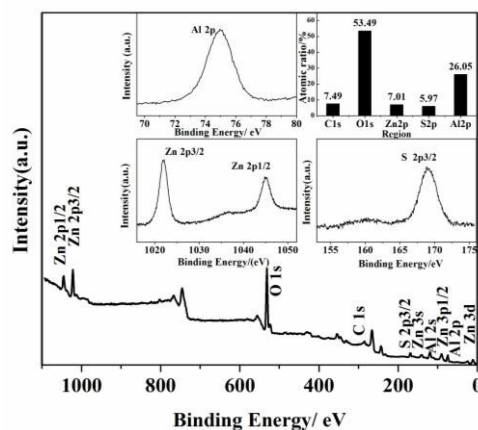
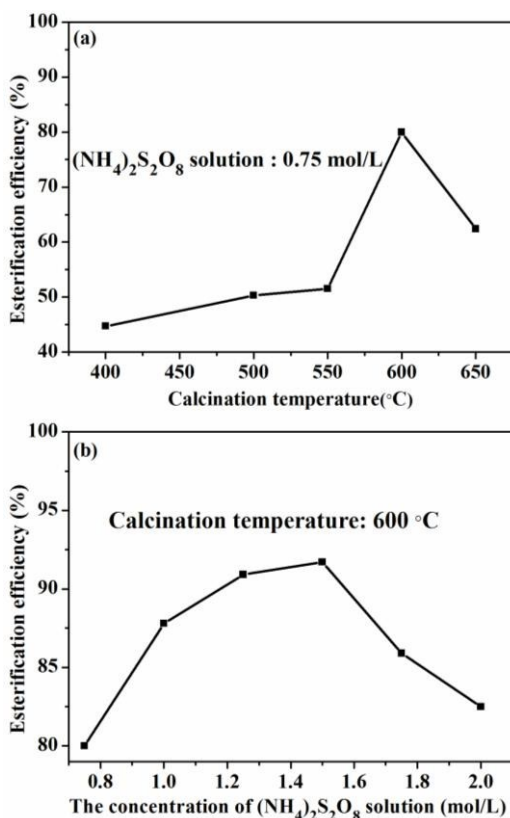


Fig. 6 XPS spectra of the  $\text{S}_2\text{O}_8^{2-}/\text{ZnAl}_2\text{O}_4$ -600. (Impregnated with 1.50 mol/L  $(\text{NH}_4)_2\text{S}_2\text{O}_8$  solution)

The near-surface chemical valence states are investigated by XPS within a range of binding energies of 0-1100 eV. Fig. 6 shows the whole XPS spectra of  $\text{S}_2\text{O}_8^{2-}/\text{ZnAl}_2\text{O}_4$ -600, revealing the strong peaks of Zn, O, C, S, and Al elements.<sup>6</sup> Among them, the observed C element is due to carbon tape from XPS instrument itself. The binding energy of Al 2p at 74.9 eV suggests the presence of  $\text{Al}^{3+}$  cation. XPS spectrum of the Zn shows two outstanding peaks are located at 1021.8 eV and 1045.2 eV, corresponding to Zn 2p<sub>3/2</sub> and Zn 2p, respectively.<sup>22</sup> In addition, the S 2p<sub>3/2</sub> peak at 168.95 eV is ascribed to the sulfur oxidation state of +6 which plays an essential role on the formation of the acidity structure.<sup>23, 24</sup> The suction-induced complex  $\text{S}=\text{O}$  improves the electron-accepting ability of the metal atoms, contributing to the formation of super acid. This result is consistent with the special bands in the range of 900-1400  $\text{cm}^{-1}$  in IR analysis. The surface sulphur content is 5.97% (atomic ratio), which is the quantitative estimated by means of XPS.

### 3.2 Catalytic performance

Fig. 7 displays the effects of the calcination temperature and impregnating concentration of the carrier on catalytic activities. These results show that the calcination temperature has a significant influence on catalytic activity. It can be observed that the  $\text{S}_2\text{O}_8^{2-}/\text{ZnAl}_2\text{O}_4$ -600 performs the highest catalytic activity with the maximum 80.0% esterification efficiency. Moreover, the results of XRD and FE-SEM show that the  $\text{S}_2\text{O}_8^{2-}/\text{ZnAl}_2\text{O}_4$ -600 possesses mesoporous structure and well crystallinity of spinel. These properties may contribute to the high catalytic activity. The influence of impregnating concentration indicates that the catalytic activities are enhanced with increasing the impregnation concentration, reaching a maximum value of 91.7% at 1.5 mol/L. However, the catalytic activities descend sharply when the concentration further increases. The reason may be that excess sulfate groups covering the surface make the acidity of solid acid decrease.<sup>25</sup> Thus an appropriate concentration of 1.5 mol/L is favorable for high catalytic activity.



**Fig. 7** The effects of the calcination temperature and impregnating concentration of the carrier on catalytic activities of  $S_2O_8^{2-}/ZnAl_2O_4$ . (The reaction condition: the molar ratio of acetic acid to *n*-butanol was 1:3; catalyst amount was 1.55 wt%; reaction time was 3h.)

**Table 2** The effect of reaction conditions on catalytic activities of  $S_2O_8^{2-}/ZnAl_2O_4-600$

Catalyst	Amount <sup>b</sup>	Time (h)	a : n <sup>c</sup> ratio	Esterification efficiency (%)
$S_2O_8^{2-}/ZnAl_2O_4-600^a$	1.55	3.0	1:1	56.1
	1.55	3.0	1:2	79.5
	1.55	3.0	1:3	91.7
	1.55	3.0	1:4	91.6
	1.55	3.0	1:5	93.0
	0.00	3.0	1:3	38.0
	0.37	3.0	1:3	76.0
	0.73	3.0	1:3	79.1
	1.14	3.0	1:3	85.4
	1.85	3.0	1:3	91.4
	2.21	3.0	1:3	91.7
	1.55	1.5	1:3	77.9
	1.55	2.0	1:3	81.3
	1.55	2.5	1:3	86.9
	1.55	3.5	1:3	91.0
1.55	4.0	1:3	91.4	
$ZnAl_2O_4-600$	1.55	3.0	1:3	45.2
$S_2O_8^{2-}/ZnAl_2O_4-600^a$ catalyst recycling experiments				
Run 1	1.55	3.0	1:3	91.7
Run 2	1.55	3.0	1:3	82.6
Run 3	1.55	3.0	1:3	72.3
Run 4	1.55	3.0	1:3	65.7
Run 5	1.55	3.0	1:3	58.9

<sup>a</sup> the synthesis condition: calcination temperature was 600 °C; the

concentration of  $(NH_4)_2S_2O_8$  solution was 1.50 mol/L.

<sup>b</sup> the amount was calculated on the basis of total weight of the reactants

<sup>c</sup> the molar ratio of acetic acid to *n*-butanol

Table 2 shows the effects of reaction conditions on catalytic activities, including the molar ratio, catalyst amount and reaction time. The molar ratio of acetic acid to *n*-butanol has a significant influence on the esterification efficiency. Stoichiometrically, the molar ratio of acetic acid to *n*-butanol is 1:1. Nevertheless, the excess *n*-butanol is used to promote the equilibrium to the direction of producing the ester. Accordingly, it is clearly seen that the esterification efficiency of  $S_2O_8^{2-}/ZnAl_2O_4-600$  increases with increasing the molar ratio of acetic acid to *n*-butanol from 1:1 to 1:3. However, a mass of *n*-butanol may dilute the concentration of acidity and slow down the reaction.<sup>26</sup> Therefore, it witnesses a slight downward trend in the esterification efficiency when the molar ratio exceeds 1:3. Therefore, the molar ratio of 1:3 is optimum to achieve a high yield.

The results of catalytic activities with the various catalyst amounts from 0 to 2.21% are demonstrated in Table 2. The esterification efficiency is 38% when the reaction is carried out without catalyst. The esterification efficiency shows an apparently upward trend with the catalyst amount increasing from 0 to 1.55 wt%. Afterward, the reaction experiences stable esterification efficiency about 91% when the catalyst amount exceeds 1.55 wt%. The reason may be that the excess acid amount might promote the reverse reaction at the mean time.<sup>27</sup> Thus, 1.55wt% is sufficient for the esterification reaction.

The effect of reaction time on the esterification efficiency is shown in Table 2. On the initial stage of 3 h, the esterification efficiency grows rapidly with prolongation of the reaction time. Within 3 h, 91.7% esterification efficiency is achieved. Then, the esterification efficiency is noticed to be stable at around 91% because of the attainment of equilibrium. The optimum reaction time is considered to be 3 h, with the maximum esterification efficiency of 91.7%.

The catalytic activity of  $ZnAl_2O_4-600$  is performed as the blank experiment. By comparison, it is found that the  $ZnAl_2O_4-600$  shows lower catalytic activity with 45.16 % efficiency. However, the  $S_2O_8^{2-}/ZnAl_2O_4-600$  catalyst exhibits high catalytic activity with above 90% efficiency.

For the recycling test, the catalyst was filtered after completion of reaction and dried at room temperature without further treatment. Then, the dried catalyst is used for the next recycling experiment with fresh reaction. As shown in Table 2, the catalyst shows an inevitable decrease in catalytic activity after 5 times recycling. The deactivation presumably is owing to the adsorption of organic groups on the surface as well as the reduction of the catalyst amount. Besides, the XRD and FT-IR analyses of the reused catalyst demonstrate that  $S_2O_8^{2-}/ZnAl_2O_4-600$  has the advantage of structure stability in recycling test.

Cite this: DOI: 10.1039/c0xx00000x

www.rsc.org/xxxxxx

ARTICLE TYPE

**Table 3** Comparison of catalytic activity of the  $\text{S}_2\text{O}_8^{2-}/\text{ZnAl}_2\text{O}_4$ -600 catalyst with other reported solid acid catalysts

Catalyst	Reaction conditions			Esterification efficiency (%)	Refs.
	a : n <sup>a</sup> ratio	amount <sup>b</sup> (wt%)	Reaction time (h)		
$\text{S}_2\text{O}_8^{2-}/\text{ZnAl}_2\text{O}_4$ -600	1:3	1.55	3	91.7	Present work
$\text{S}_2\text{O}_8^{2-}/\text{ZnO}$ -600	1:3	1.55	3	52.9	Present work
$\text{S}_2\text{O}_8^{2-}/\text{Al}_2\text{O}_3$ -600	1:3	1.55	3	79.3	Present work
$\text{S}_2\text{O}_8^{2-}/\text{ZrO}_2$	1:3	12	2	91.8	[28]
$\text{S}_2\text{O}_8^{2-}/\text{ZrO}_2$ - $\text{CeO}_2$	1:3	12	2	96.6	[28]
sulfated $\text{TiO}_2$	1:1.2	12.09	2.5	92.2	[29]
$\text{SO}_4^{2-}-\text{TiO}_2$	1:3	2	0.75	60.1	[30]
$\text{SO}_4^{2-}-\text{Ce}_{0.02}/\text{TiO}_2$	1:3	2	0.75	97.1	[30]
$\text{SO}_4^{2-}/\text{TiO}_2$ -Zr-La	1:1.56	4.88	0.5	85	[31]
$\text{Ti}(\text{SO}_4)_2$	1:0.69	5.15	2	90.22	[32]
S- $\text{TiO}_2/\text{MCM-41}$	1:0.69	5.15	2	87.62	[32]

<sup>a</sup> The molar ratio of acetic acid to *n*-butanol<sup>b</sup> Catalyst amount is calculated on the basis of total weight of the reactants

Table 3 shows the comparison of  $\text{S}_2\text{O}_8^{2-}/\text{ZnAl}_2\text{O}_4$ -600 with  $\text{S}_2\text{O}_8^{2-}/\text{ZnO}$ -600,  $\text{S}_2\text{O}_8^{2-}/\text{Al}_2\text{O}_3$ -600 and other reported solid acid catalysts. The  $\text{S}_2\text{O}_8^{2-}/\text{ZnAl}_2\text{O}_4$ -600 catalyst perform the higher catalytic activity than the  $\text{S}_2\text{O}_8^{2-}/\text{ZnO}$ -600 and  $\text{S}_2\text{O}_8^{2-}/\text{Al}_2\text{O}_3$ -600 catalyst with simple oxide carrier. The catalytic activity of  $\text{S}_2\text{O}_8^{2-}/\text{ZnAl}_2\text{O}_4$ -600 is comparable with the series of  $\text{SO}_4^{2-}/\text{TiO}_2$  and  $\text{SO}_4^{2-}/\text{ZrO}_2$  catalysts in esterification reactions.<sup>28-32</sup> However, crystal structure transformation was commonly observed in the synthesis and modification of  $\text{SO}_4^{2-}/\text{TiO}_2$  and  $\text{SO}_4^{2-}/\text{ZrO}_2$ , which affected their catalytic performances.<sup>3,4</sup> Notably,  $\text{ZnAl}_2\text{O}_4$  as a new carrier of solid acid exhibits the advantages of the simpler crystal and excellent crystal structure stability in present work.

## Conclusions

A series of  $\text{S}_2\text{O}_8^{2-}/\text{ZnAl}_2\text{O}_4$ -*T* with spinel structure was successfully prepared by sol-gel method. It can be found that the catalytic behaviors were dramatically affected by the calcination temperature. The  $\text{S}_2\text{O}_8^{2-}/\text{ZnAl}_2\text{O}_4$ -600 catalyst showed the highest activity. With the molar ratio of acetic acid to *n*-butyl alcohol of 1:3, the catalyst amount of 1.55wt% and reaction time of 3 h, the esterification efficiency of  $\text{S}_2\text{O}_8^{2-}/\text{ZnAl}_2\text{O}_4$ -600 reached the maximum 91.7%. The characterizations revealed that the  $\text{ZnAl}_2\text{O}_4$  carrier had the prominent advantages of single crystal shape and stable structure in the process of sulfidation and recycling test.  $\text{S}_2\text{O}_8^{2-}/\text{ZnAl}_2\text{O}_4$ -600 showed mesoporous structures, which may be contributed to high catalytic activity. In conclusion,  $\text{ZnAl}_2\text{O}_4$  can be used as a promising carrier for the investigation in solid acid.

## Acknowledgments

The authors gratefully acknowledge the financial support from NSFC (Nos. 21203170 and 41472042) and the National College

Students' Innovative Training Program (Nos. 201410491024 and 201310491019), the Fundamental Research Funds for National University (No. 1410491B04) and TLOFCUG (No. SKJ 2013008).

### Notes and references

<sup>a</sup> Faculty of Materials Science and Chemistry, Engineering Research Center of Nano-Geomaterials of Ministry of Education, China University of Geosciences, Wuhan 430074, China. E-mail address: jxwyqh@sina.com Tel/ fax: +86-27-87407079

- F. Su and Y.H. Guo, *Green Chem.*, 2014, **16**, 2934-2957.
- H. Zhao, P.P. Jiang, Y.M. Dong, M. Huang and B.L. Liu, *New J. Chem.*, 2014, **38**, 4541-4548.
- L. Li, S.W. Liu, J.M. Xu, S.T. Yu, F.S. Liu, C.X. Xie, X.P. Ge and J.Y. Ren, *J. Mol. Catal. A: Chem.*, **368-369** (2013) 24-30.
- D.H. Guan, M.Q. Fan, J. Wang, Y. Zhang, Q. Liu and X. Y. Jing, *Mater. Chem. Phys.*, **122** (2010) 278-283.
- G.D. Yadav and R.V. Sharma, *J. Catal.*, **311** (2014) 121-128.
- Z.R. Zhu, X.Y. Li, Q.D. Zhao, S.M. Liu, X.J. Hu and G.H. Chen, *Mater. Lett.*, **65** (2011) 194-197.
- T.M. Sankaranarayanan, R.V. Shanthi, K. Thirunavukkarasu, A. Pandurangan and S. Sivasanker, *J. Mol. Catal. A: Chem.*, **379** (2013) 234-242.
- Z.R. Zhu, Q.D. Zhao, X.Y. Li, H. Li, M. Tade and S.M. Liu, *Catal. Sci. Technol.*, **3** (2013) 788-796.
- K. Yan, X. Wu, X. An and X.M. Xie, *J. Alloys Comp.*, **552** (2013) 405-408.
- S.V. Jadhav, K.M. Jinka and H.C. Bajaj, *Catal. Today.*, **198** (2012) 98-105.
- D.J. Lin, S.F. Shen, H.B. Pan and N.S. Chen, *Chinese J. Inorg. Chem.*, **16** (2000) 757-762.
- J.X. Wang, H. Pan, D.W. Meng, X.L. Wu, Y.Q. Wang and X. Meng, *React. Kinet. Catal. Lett.*, **102** (2011) 331-341.
- L. Chen, J.X. Wang, D.W. Meng, H. Pan, G.H. Su, Y. Xiao and Z.F. Yan, *React. Kinet. Catal. Lett.*, **109** (2013) 575-587.
- H. Pan, J.X. Wang, L. Chen, G.H. Su, J.M. Cui, D.W. Meng and X.L. Wu, *Catal. Commun.*, **35** (2013) 27-31.

- 15 K.H. Jiang, D.M. Tong, J.Q. Tang, R.L. Song and C.W. Hu, *Appl. Catal. A: Gen.*, **389** (2010) 46-51.
- 16 R.P. Yao, M.J. Zhang, J. Yang, D.L. Yi, J. Xu, F. Deng, Y. Yue and C.H. Ye, *Aata Chim. Sinica*, **63** (2005) 269-273.
- 5 17 S. Farhadi and S. Panahandehjoo, *Appl. Catal. A: Gen.*, **382** (2010) 293-302.
- 18 B.B. Chang, J. Fu, Y.L. Tian and X.P. Dong, *Appl. Catal. A: Gen.*, **437-438** (2012) 149-154.
- 19 V.G. Deshmane and Y.G. Adewuyi, *Appl. Catal. A: Gen.*, **462-463** (2013) 196-206.
- 10 20 P.F. Chen, M.X. Du, H. Lei, Y. Wang, G.L. Zhang, F.B. Zhang and X.B. Fan, *Catal. Commun.*, **18** (2012) 47-50.
- 21 C.C. Hwang and C.Y. Mou, *Appl. Catal. A: Gen.*, **365** (2009) 173-179.
- 15 22 L.J. Liu, G.L. Zhang, L. Wang, T. Huang and L. Qin, *Ind. Eng. Chem. Res.*, **50** (2011) 7219-7227.
- 23 C.W. Dunnill, Z.A. Aiken, A. Kafizas, J. Pratten, M. Wilson, D.J. Morgan and I.P. Parkin, *J. Mater. Chem.*, **19** (2009) 8747-8754.
- 24 L.G. Devi, R. Kavitha, *Mater. Chem. Phys.* **143** (2014) 1300-1308.
- 20 25 C.H. Li, Y.X. Zhao and B. Dai, *J. Ind. Eng. Chem.*, **18** (2012) 520-525.
- 26 G. Kuriakose and N. Nagaraju, *J. Mol. Catal. A: Chem.*, **223** 2004 155-159.
- 27 T.F. Parangi, B.N. Wani and U.V. Chudasama, *Ind. Eng. Chem. Res.*, **52** (2013) 8969-8977.
- 25 28 G.D. Fan, M. Shen, Z. Zhang and F.R. Jia, *J. Rare Earth.*, **27** (2009) 437-442.
- 29 H. Zhao, P.P. Jiang, Y.M. Dong, M. Huang and B.L. Liu, *New J. Chem.*, **38** 2014 4541-4548.
- 30 30 G. Xiao, J.F. Zhou, X. Huang, X.P. Liao and B. Shi, *RSC Adv.*, **4** 2014 4010-4019.
- 31 W.P. Shi, *Catal. Lett.*, **143** (2013) 732-738.
- 32 Y.H. Wang, Y.T. Gan, R. Whiting and G.Z. Lu, *J. Solid State Chem.*, **182** (2009) 2530-2534